NRL Report 7814

Spreading of Waves Launched by ELF/VLF Satellite

FRANCIS J. KELLY, DENNIS J. BAKER,
AND GERALD A. CHAYT

Electromagnetic Propagation Branch
Communications Sciences Division

December 31, 1974

NAVAL RESEARCH LABORATORY
Washington, D.C.

SECURITY CLASSIFICATION OF THIS PAGE *(When Data Entered)*

REPORT DOCUMENTATION PAGE

READ INSTRUCTIONS BEFORE COMPLETING FORM

1. REPORT NUMBER: NRL Report 7814	2. GOVT ACCESSION NO.
3. RECIPIENT'S CATALOG NUMBER	
4. TITLE *(and Subtitle)*: SPREADING OF WAVES LAUNCHED BY AN ELF/VLF SATELLITE	5. TYPE OF REPORT & PERIOD COVERED: Interim report on a continuing NRL problem
	6. PERFORMING ORG. REPORT NUMBER
7. AUTHOR(s): Francis J. Kelly, Dennis J. Baker and Gerald A. Chayt	8. CONTRACT OR GRANT NUMBER(s)
9. PERFORMING ORGANIZATION NAME AND ADDRESS: Naval Research Laboratory, Washington, D.C. 20375	10. PROGRAM ELEMENT, PROJECT, TASK AREA & WORK UNIT NUMBERS: NRL Problem R07-30, RF 21-222-401-4360
11. CONTROLLING OFFICE NAME AND ADDRESS: Department of the Navy, Office of Naval Research, Arlington, Virginia 22217	12. REPORT DATE: December 31, 1974
	13. NUMBER OF PAGES: 29
14. MONITORING AGENCY NAME & ADDRESS*(if different from Controlling Office)*	15. SECURITY CLASS. *(of this report)*: Unclassified
	15a. DECLASSIFICATION/DOWNGRADING SCHEDULE

16. DISTRIBUTION STATEMENT *(of this Report)*

Approved for public release; distribution unlimited.

17. DISTRIBUTION STATEMENT *(of the abstract entered in Block 20, if different from Report)*

18. SUPPLEMENTARY NOTES

19. KEY WORDS *(Continue on reverse side if necessary and identify by block number)*

Electromagnetic propagation	Ray tracing
ELF transmission	Satellite transmission
Ionosphere	VLF transmission
Magnetosphere	Whistler waves

20. ABSTRACT *(Continue on reverse side if necessary and identify by block number)*

Radio signals from an ELF/VLF transmitting satellite may be propagated through the ionosphere to receiving antennas on the earth's surface. Among many factors important in estimating the received signal strength is the geometric spreading factor, $d\Omega/dA_E$, measuring the area, dA_E, of the earth's surface intercepting the power radiated into the solid angle, $d\Omega$, from the satellite. The spreading factor has been isolated and accurately estimated by a ray-tracing computer program. Calculations have been performed for transmissions at 3 and 10 kHz and for three different ionospheric models using satellite altitudes ranging

(continued)

20. Abstract (Continued)

between 300 and 8000 km for some representative receiver point locations. Spreading factors were calculated both for direct and multiple hop waves in the earth-ionosphere waveguide. For low satellite altitudes (below about 2200 km) the coverage patterns of spreading factor versus the receiver's geographic position showed well-defined peaks, indicating locally high radio fields. For higher altitudes the coverage patterns were broader but showed weaker maximum field strengths. A comparison was made with a simply estimated factor employed by Smith and Rorden, and quantitative and qualitative differences are noted.

CONTENTS

SPREADING OF WAVES LAUNCHED BY AN ELF/VLF SATELLITE

BACKGROUND

In calculating a signal-to-noise power budget for a satellite-borne transmitter operating in the extremely low frequency (ELF) or very low frequency (VLF) range, it is necessary to calculate the geometric spreading factor of the waves as they propagate from a source in the ionosphere to a receiver at the earth's surface. This spreading factor is the ratio of an element of solid angle $d\Omega$ measured at the satellite transmitter to an element of area dA_E at the surface of the earth; these are related in such a way that the power radiated by the satellite into the angle $d\Omega$ falls incident eventually at the earth's surface in the element of area dA_E (see Fig. 1). In producing a complete signal level prediction from a given transmitter, additional important factors must be evaluated, such as the antenna radiated power pattern, the ionospheric transmission and reflection coefficients, and the transmission coefficient of the sea surface (taking polarization into account). These terms and their combination to provide a total power budget will be treated in subsequent reports. The objective of this report is to describe a technique for evaluating the spreading factor and to present examples of calculated results. In the Theory section, we will describe more fully the background for this type of calculation and give a procedure for evaluating the elements of solid angle and area that uses a computer program which integrates the Haselgrove differential equations. In the section on Calculations and Results, we will describe some calculations and results obtained with several frequencies, transmitter locations and ionospheric models.

THEORY

Geometrical Optics

The geometrical optical approach for the calculation of field strengths has been used previously in studies of electromagnetic wave propagation. Many works [1-11] discuss or apply this approach to calculating electromagnetic field strengths. In particular, Refs. 2 and 3 treat the case of passage at a plane boundary from a medium with a high index of refraction, such as the ionosphere, abruptly into one with a low index of refraction, such as free space below the ionosphere. The idealized propagation problem is formulated exactly in terms of separable wave functions in cylindrical coordinates. References 2 and 3 show that the integral expression thus obtained may be evaluated by the method of steepest descents and that the first term in the evaluation of the wave fields is identical to the expression given by geometrical optics. (By *geometrical optics* we mean that the resultant field amplitude is given by the product of an antenna radiation pattern factor, a spreading factor computed according to geometric optic ray tracing

Manuscript submitted August 19, 1974.

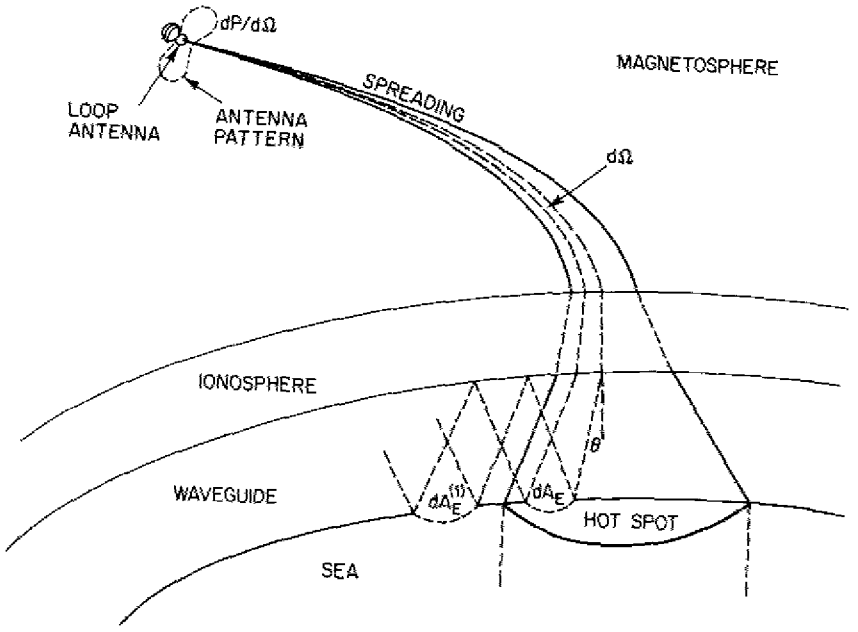

Fig. 1 — Spreading factor quantities $d\Omega$ and dA_E. The multihop area element $dA_E^{(1)}$ is also shown

(i.e., Snell's law at sharp boundaries) and appropriate plane-wave reflection and/or transmission factors that account for the reflection and/or transmission losses occurring at sharp boundaries.)

Reference 2 shows that higher order terms represent lateral wave, surface wave, and evanescent wave contributions and presents an analytic propagation solution both for an isotropic medium and a uniaxially anisotropic medium. The equivalence of a geometric optics formulation and the saddlepoint evaluation of the exact integral formulation is not shown for the general anisotropic medium (possibly because the separation of variables technique is not usable in the general anisotropic case). Nevertheless, we will use the geometric optics spreading term in our power budget because it has strong support from physical intuition; it is common scientific practice to do so in treating whistlers [9], and it has firm theoretical justification in the limited cases where exact theoretical field evaluations can be obtained and evaluated by a saddlepoint technique.

The Ray Tracing Program

Alexander [12] describes a ray tracing computer program that integrates the three-dimensional Haselgrove equations [13] along a ray path in the magnetosphere. The Haselgrove equations are reviewed by Budden [14]. The six Haselgrove equations are given below in the notation of Ref. 12:

$$\dot{r} = \frac{1}{\mu^2}\left(\rho_r - \mu \frac{\partial \mu}{\partial \rho_r}\right) \tag{1}$$

$$\dot{\theta} = \frac{1}{r\mu^2}\left(\rho_\theta - \mu \frac{\partial \mu}{\partial \rho_\theta}\right) \tag{2}$$

$$\dot{\varphi} = \frac{1}{r\mu^2 \sin\theta}\left(\rho_\varphi - \mu \frac{\partial \mu}{\partial \rho_\varphi}\right) \tag{3}$$

$$\dot{\rho}_r = \frac{1}{\mu}\frac{\partial \mu}{\partial r} + \rho_\theta \dot{\theta} + \rho_\varphi \sin\theta \dot{\varphi} \tag{4}$$

$$\dot{\rho}_\theta = \frac{1}{r}\left(\frac{1}{\mu}\frac{\partial \mu}{\partial \theta} - \rho_\theta \dot{r} + r\cos\theta \rho_\varphi \dot{\varphi}\right) \tag{5}$$

$$\dot{\rho}_\varphi = \frac{1}{r\sin\theta}\left(\frac{1}{\mu}\frac{\partial \mu}{\partial \varphi} - \rho_\varphi \sin\theta \dot{r} - r\cos\theta \rho_\varphi \dot{\theta}\right). \tag{6}$$

In these equations r, θ, and φ are the spherical coordinates of the ray position and μ is the phase refractive index. The quantities ρ_r, ρ_θ, and ρ_φ are the components of the wave normal vector $\underline{\rho}$ which has magnitude μ. (In other words the vector $\underline{\rho}$ at a point on the ray trace has the direction of the phase velocity of the wave and its magnitude equal to the wave's phase refractive index.) The quantities $\dot{r}$, $\dot{\theta}$, $\dot{\varphi}$, $\dot{\rho}_r$, $\dot{\rho}_\theta$, and $\dot{\rho}_\varphi$ are the derivatives of the above quantities with respect to the speed of light times time (ct). During the computer calculation the above differential equations are integrated using a Runge-Kutta-Gill technique [15] and an Adams-Bashford technique [12].

Magnetospheric and Ionospheric Models

A magnetospheric ion and electron density model is used during a ray trace for the calculation of the refractive index μ of a wave located at a given point (r, θ, φ) in the magnetosphere with the wave's phase velocity pointing in a particular direction. It is also required for determining the partial derivatives $\partial\mu/\partial\theta$, $\partial\mu/\partial\rho_\theta$, etc., also used in the Haselgrove equations. The program has the option of using any of five different magnetospheric models. The inclusion of additional magnetospheric models is a straightforward computer programming problem.

A model of the lower ionosphere below 300 km was not included in the original program, and all ray traces performed by Alexander were originated and ended at heights at or above 300 km. For tracing rays at altitudes below 300 km, additional programming was included to account for the ionospheric electron and ion densities below 300 km. Three different electron and ion density models have been used in this height range. The values of $d\Omega/dA_E$ do not seem to be very sensitive to the choice of lower ionospheric electron density profile. Specific details regarding the three models (referred to as A-1, A-2, and A-3) are contained in the Appendix.

Evaluation of Direct Spreading Factor

In performing a calculation of $d\Omega/dA_E$ from a satellite at a fixed location, an initial starting direction is chosen for the wave propagation vector $\underline{\rho}$, and a ray trace is performed down to the earth's surface. (Sometimes the ray does not reach the earth's surface because it reflects at some point high in the ionosphere, or because it totally reflects at the lower boundary of the ionosphere.) Providing the ray reaches the ground, the location on the earth's surface at which it intercepts the ground is stored for future use. The second and third rays are then initiated at the satellite, with slightly different initial directions. The locations at which these rays intercept the earth's surface are also stored. From the directions of the three rays, a solid angle element $d\Omega$ is determined. From the locations of the three corresponding points on the earth's surface, an area element dA_E is determined. By this method, the ratio $d\Omega/dA_E$ is constructed.

Evaluation of Multiple Hop Spreading Factor

When the program is run in its multihop mode, it is necessary to reverse the sign of ρ_r for each of the initial rays at the point where it first intersects the earth's surface and to send it back toward the ionosphere. When each ray trace reaches a reference level (approximately 70 km) near the bottom of the ionosphere, the sign of ρ_r is reversed again and the ray is headed back to the earth's surface. The coordinates of the second point of ground intersection of each ray are noted and stored. From the locations at which the three rays have intercepted the earth's surface after one reflection from the earth and one reflection at the ionosphere, the ratio $d\Omega/dA_E^{(1)}$ is formed. Likewise after n reflections at the ground and ionosphere, the ratio $d\Omega/dA_E^{(n)}$ is formed.

At each reflection at the ionosphere, portions of the wave power will be transmitted, reflected, and absorbed. These losses must be accounted for in a total power budget, but are not a part of the spreading factor.

At first glance one might doubt the applicability of a geometric optics formulation to a case in which the waveguide height is on the order of a wavelength. However, Galejs (Ref. 5, pages 125-127) shows that the method of images (or essentially, geometric optics) gives results in close agreement with exact wave theoretic calculations for both VLF and ELF waves within 1000 km of a transmitter. In our formulation we have omitted the induction field terms kept by Galejs and retain only the radiation field terms. The induction field terms should become significant only when the free-space wavelength exceeds 2π times the slant range from the ionospheric exit point to the receiver. For an ionospheric height of 70 km the inductive term would not be important for frequencies above 700 Hz.

Evaluation of $d\Omega$

In determining the initial wave direction of a ray trace, Alexander's program employs two variables, DELI and DELPHI. These correspond to the angles δ_θ and δ_φ in Fig. 2, which shows a coordinate frame with unit vectors $\hat{r}, \hat{\theta}, \hat{\varphi}$ with its origin at the satellite's location. The unit vector $\hat{r}$ is pointed in the radial direction (away from the center of

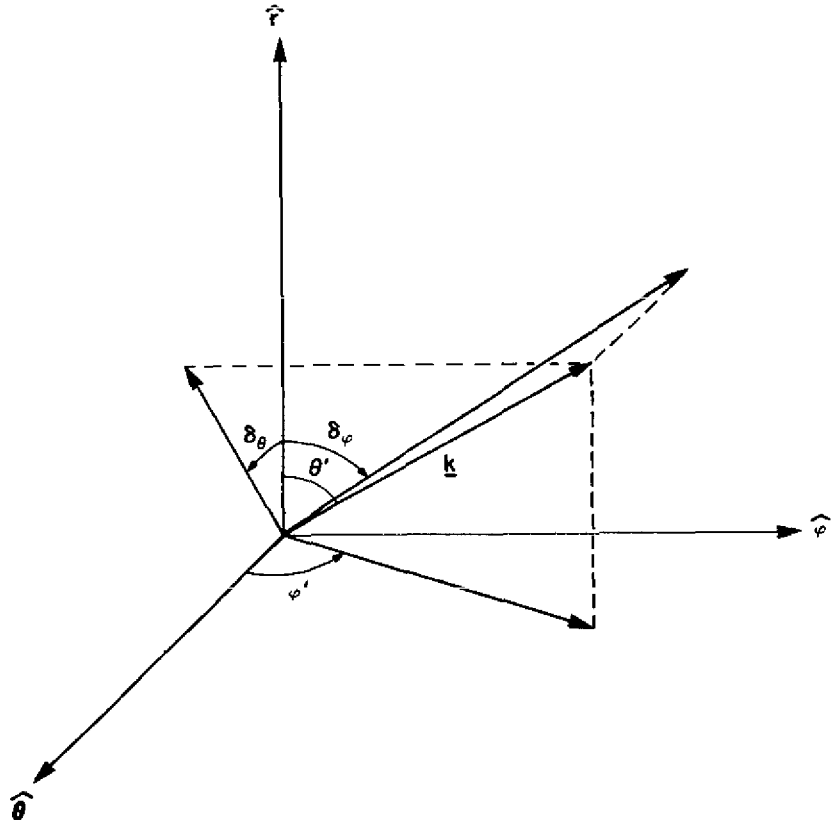

Fig. 2 — Propagation wave angles showing relation of angles δ_θ and δ_φ to spherical polar angles (θ', φ')

the earth). The unit vector $\hat{\theta}$ is perpendicular to $\hat{r}$, lies in the plane of the meridian and points southward; the unit vector $\hat{\varphi}$ is orthogonal to both $\hat{r}$ and $\hat{\theta}$ and points eastward. The angle δ_θ is the angle between the $\hat{r}$ vector and the projection of the wave propagation vector $\underline{k}$ onto the plane of the meridian (the $\hat{r}$, $\hat{\theta}$ plane). The angle δ_φ is the angle between the $\hat{r}$ vector and the projection of the wave propagation vector $\underline{k}$ onto the ($\hat{r}$, $\hat{\varphi}$) plane. The transformation between the angles (δ_θ, δ_φ) to a θ', φ' direction in a spherical coordinate system having the same origin is given by

$$\tan \varphi' = \tan \delta_\varphi \cot \delta_\theta \tag{7}$$

$$\sin \theta' = \left(\frac{\cos^2 \delta_\varphi \sin^2 \delta_\theta + \sin^2 \delta_\varphi \cos^2 \delta_\theta}{1 - \sin^2 \delta_\theta \sin^2 \delta_\varphi} \right)^{1/2} . \tag{8}$$

The differential element of solid angle $d\Omega$ is well known in the spherical coordinate system as

$$d\Omega = \sin \theta' \, d\theta' \, d\varphi'. \tag{9}$$

The differential angle product $d\theta' \, d\varphi'$ is related to the angular product $d\delta_\theta \, d\delta_\varphi$ by the Jacobian of the transformation given by Eqs. (7) and (8);

$$d\theta' \, d\varphi' = \left| \frac{\partial \, (\theta', \varphi')}{\partial \, (\delta_\theta, \delta_\varphi)} \right| \, d\delta_\theta \, d\delta_\varphi, \tag{10}$$

where the Jacobian is defined by

$$\frac{\partial(\theta', \varphi')}{\partial(\delta_\theta, \delta_\varphi)} = \frac{\partial\theta'}{\partial\delta_\theta} \frac{\partial\varphi'}{\partial\delta_\varphi} - \frac{\partial\theta'}{\partial\delta_\varphi} \frac{\partial\varphi'}{\partial\delta_\theta} . \tag{11}$$

Evaluating the partial derivatives of Eq. (11) using Eqs. (7) and (8), and combining Eqs. (9), (10), and (11), we obtain

$$d\Omega = \frac{\cos \delta_\theta \, \cos \delta_\varphi}{(1 - \sin^2 \delta_\theta \, \sin^2 \delta_\varphi)^{3/2}} \, d\delta_\theta \, d\delta_\varphi . \tag{12}$$

This expression can be used to evaluate the solid angle made by three intersecting rays at the transmitter (satellite).

Evaluation of dA_E

When the ray path integration finally reaches the earth's surface, the integration stops. The values for the latitude Θ and longitude Φ of the point where the earth's surface is intercepted are determined by linearly interpolating between the coordinates of two points that straddle the earth's surface — one slightly above it and one slightly below it. Similarly, we evaluate the coordinates (Θ_2, Φ_2) and (Θ_3, Φ_3), the ground intersection points of the second and third ray traces. From these three landing points an element of area dA_E is then computed according to

$$dA_E = a^2 \, \beta_{21} \, \beta_{31} \, \left| \sin (\gamma_{21} - \gamma_{31}) \right| , \tag{13}$$

where a is the radius of the earth, and

$$\beta_{21}{}^2 = (\Theta_1 - \Theta_2)^2 + \sin^2 [(\Theta_1 + \Theta_2)/2] \, (\Phi_1 - \Phi_2)^2 \tag{14}$$

$$\beta_{31}{}^2 = (\Theta_1 - \Theta_3)^2 + \sin^2 [(\Theta_1 + \Theta_3)/2] \, (\Phi_1 - \Phi_3)^2 \tag{15}$$

$$\tan \gamma_{21} = \frac{\Theta_1 - \Theta_2}{\sin [(\Theta_1 + \Theta_2)/2] (\Phi_1 - \Phi_2)} \tag{16}$$

$$\tan \gamma_{31} = \frac{\Theta_1 - \Theta_3}{\sin [(\Theta_1 + \Theta_3)/2] (\Phi_1 - \Phi_3)} . \tag{17}$$

The above algorithm [Eqs. (13)—(17)] treats the small area on the spherical earth's surface as if it were a plane area (which is a very good approximation since $dA_E \ll a^2$). The calculation of dA_E for multihop waves is done likewise by applying Eq. (13) to the coordinates of the ground interception points of the multihop wave.

CALCULATIONS AND RESULTS

Ray Tracing Through the Magnetosphere

Ray Traces at 3 kHz — Using the winter nighttime magnetospheric model, we calculated propagation paths for 3-kHz waves initiated at 300-km height having their wave normals directed vertically outward from the center of the earth at each 5° in magnetic dipole latitude in the range 20°N to 55°N. An earth-centered geomagnetic dipole field model was used. The ray tracing paths are shown in Fig. 3. Each ray is terminated at its reflection point (the point at which the ray would reverse its direction and return toward the northern hemisphere). We may note that none of these rays propagate to the earth's surface in the southern hemisphere. (The actual occurrence of lightning-induced, ground-to-ground whistlers at this frequency is commonly attributed to the occurrence of ducts, i.e., localized enhancements of electron and ion density along a magnetic field line.)

Downgoing Ray Traces — Several reversed rays (Fig. 4) were initiated near the reflection point of the 3-kHz ray which originally was an upgoing ray originated at 45°N latitude. The wave normal directions were reversed nearly 180° from that of the ray traced in Fig. 3, so the downcoming rays nearly retraced the path of the upgoing ray back towards the earth's surface in the northern hemisphere. The center ray shown in Fig. 4 has its wave normal directed vertically inward toward the center of the earth when it reaches the altitude 300 km. The other two rays are started with wave normals directed ±0.25° with respect to the center ray. These rays reach 300 km with a spread of approximately 3.5° in latitude. The spreading is not uniform, however, with the inner ray landing approximately 1° south of the center ray, and the outer ray landing approximately 2.5° north of the center ray. All the rays shown in Fig. 4 obey Snell's law for propagation into the earth-ionosphere waveguide.

Propagation Through Various Regimes — During the propagation of a 3-kHz wave from a source in the magnetosphere to the earth's surface, it is quite possible for the wave to pass from a region in which the index of refraction surface is closed to one in which the surface is open and vice versa. Usually this does not produce a strong effect on the propagation of the wave (unless the wave normal is nearly transverse to the magnetic field).

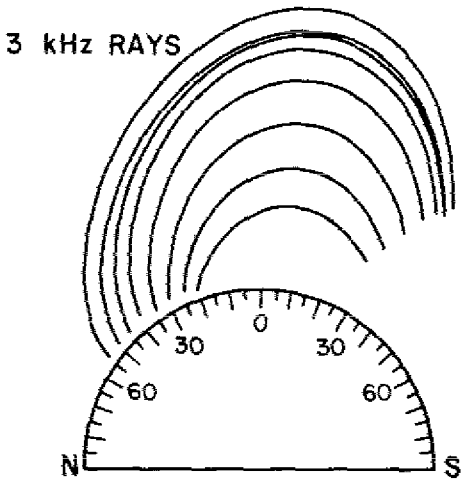

Fig. 3 — Upgoing ray tracings at 3 kHz using a winter nighttime magnetospheric model. The rays are arbitrarily terminated at their reflection points.

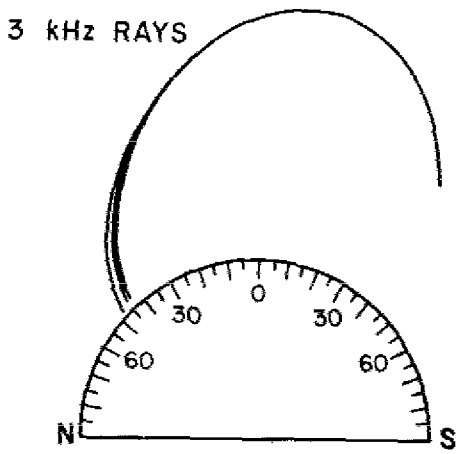

Fig. 4 — Downward ray traces from a satellite position near the reflection point. The traces show nonsymmetrical N-S spreading about the central ray.

For example, the 3-kHz wave illustrated in Fig. 5 passes smoothly from its origin in the southern magnetosphere to its arbitrary termination 300 km above the earth at 45°N latitude even though it proceeds from a region in which it has a closed index of refraction surface (solid line portion of path) to an open surface region (dashed line portion of the path) and back to a closed surface region. These topological transitions are discussed by Stix [16].

Frequency Variation of Ray Trajectories — The frequency dependence of the ray paths of waves propagating in the magnetosphere may permit some aiming of the signal. Figure 6 shows that there is an extended region of the southern magnetosphere from which waves in the band from 700 Hz to 30 kHz can propagate to the 45°N latitude receiver location. In principle, a satellite transmitter having a range of transmitted frequencies between 700 Hz and 30 kHz in a circular polar orbit at an altitude of 8000 km (dashed line on Fig. 6) could be in radio contact with a point at 45°N latitude for a period of about 25 min out of an orbital period of 283 min. However, this technique must be regarded only as an interesting theoretical possibility because its implementation would require that the transmitter possess fairly detailed information about the intervening magnetoplasma densities, so that it can select a proper frequency variation with time during its orbital pass. One approach would have a feedback signal from the communication reception area sent to the satellite (perhaps via UHF) to control automatically the satellite's frequency to produce the best reception.

Figure 6 also implies that a transmitter located in the same hemisphere as the receiver at altitudes less than a few thousand kilometers would not ordinarily gain very much signal aiming flexibility from frequency diversity because all of the rays from 700 Hz to 30 kHz appear to follow nearly the same ray path through the lower magnetosphere down to 300 km.

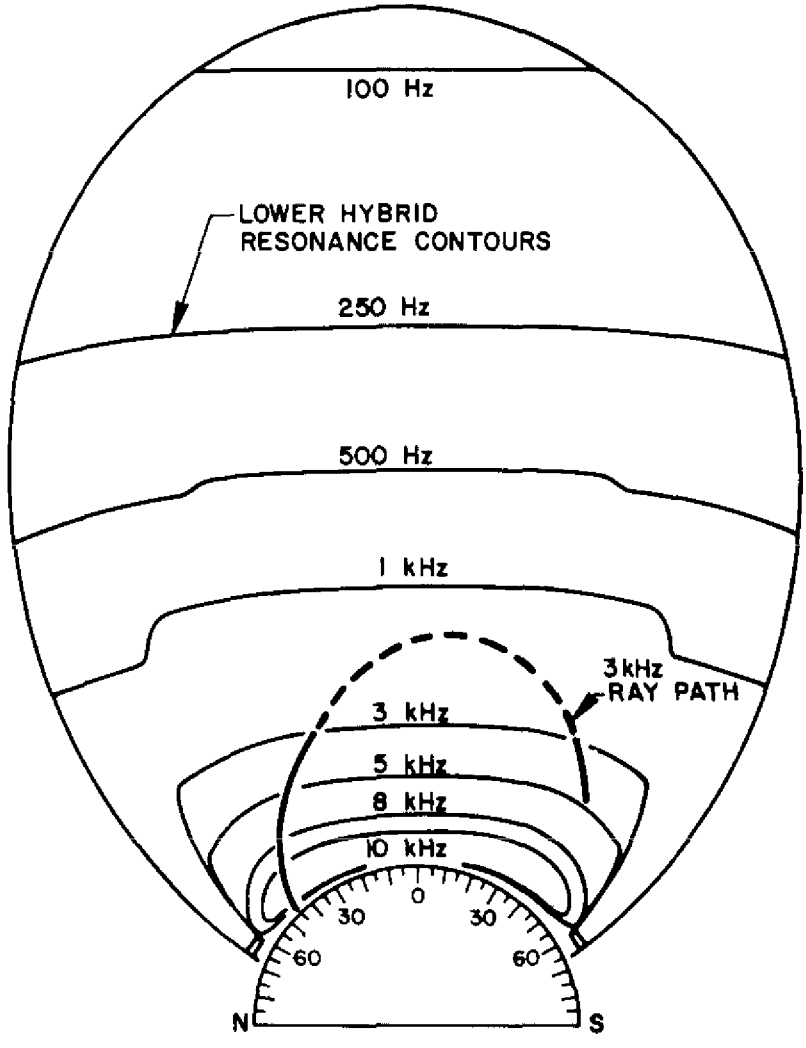

Fig. 5 — A 3-kHz ray path shown crossing twice through the 3-kHz lower hybrid resonance frequency regime. The refractive index surface is open along the dashed portion of the ray path and closed along the solid line portion.

Ray Tracing Through the Lower Ionsophere — As mentioned previously, the computer program employs a Runge-Kutta technique to initiate the numerical integration and the Adams-Bashford technique to carry out the main bulk of the integration of the Haselgrove equations. The Adams-Bashford predictor-corrector integration technique computes the new value of the coordinates from a knowledge of the values of the coordinates and derivatives at previous points in the integration. When the predicted values of the coordinates differ appreciably from the corrected values, the program reduces the integration step size by one-half and recomputes the coordinates. When the program is tracing rays through a boundary where one electron density model (the magnetosphere) abuts another (the lower ionosphere), it is essential that the two models join continuously to keep the difference between the predicted and corrected values of the coordinates

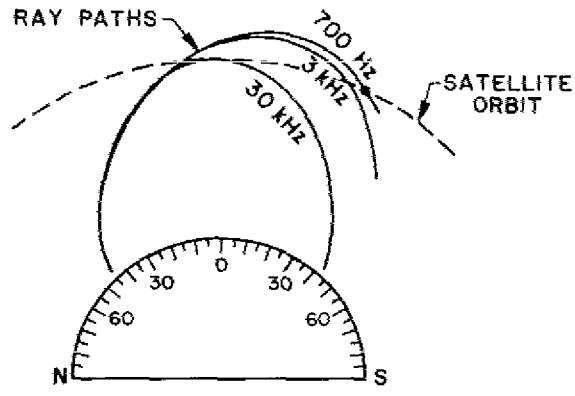

Fig. 6 — Upgoing ray traces at several frequencies illustrating the aiming flexibility of a very wide-band, frequency-agile satellite

small in going across the boundary. In implementing lower ionospheric models A-1 and A-2 in the computer, a brute force method was used to effect the joining between the two plasma regions; i.e., the electron and ion densities at 300 km were set equal to whatever value they had at the last integration location above 300 km. This *ad hoc* selection of the 300-km electron and ion densities causes the predictor-corrector comparator to halve the step size repeatedly as it tries to pass 300-km height. With sufficiently small step size, the change in electron densities between the points that straddle the 300-km height becomes insignificant. The program can then pass through the 300-km level and proceed to lower altitudes where the electron and ion density profiles are described by smoothly varying functions of the coordinates. In this lower region the predictor-corrector notices that very little error is being made and permits the step size to grow larger. Thus, in using models A-1 or A-2, the program halves the step size as the ray nears the "barrier" at 300 km.

Below 300 km the program doubles the step size rapidly, and the integration automatically speeds up. With model A-1, the program slows down again as the ray height approaches 70 km. To facilitate the ray tracing, the calculation is stopped at 71.0-km height, and a new ray is initiated at 69.9 km having the correct wave normal direction for propagation in the earth-ionosphere waveguide (if the wave normal angle at 71.0 km is less than the critical angle for exiting from the ionosphere). If at 71.0 km the wave normal angle is greater than the critical angle for exiting into the waveguide, total internal reflection is assumed to occur, and the ray tracing is halted.

Usually a ray that exits from the lower ionosphere will continue down to the earth's surface. However, rays that exit from the ionosphere at an angle from the normal exceeding about 80° will not intersect the earth's surface, but will propagate in a straight line and intersect the lower ionosphere again. Because there is no way to form an element of area dA_E by using these rays, the ray tracing is terminated when the computer notices that the radial coordinate of the wave is increasing before a ground reflection takes place.

With model A-2, the integration through the lower ionosphere is slower because there are numerous boundaries at which the derivatives of electron density are discontinuous. In model A-2 the computer permits the ray to emerge from the lower ionosphere at 84 km.

Spreading Factor Results

Figure 7 shows the variation of the spreading factor with receiver latitude for 3-kHz waves from a fixed satellite transmitter. Two different transmitter locations and two different lower ionospheric models are used. Figure 8 shows the variation of the spreading factor with the longitude of the receiver using lower ionospheric model A-1. (Actually, in performing the latter calculations, δ_φ was varied while δ_θ was held fixed at the transmitter. This procedure resulted in a relatively large change in the longitude of the ground receiver point and only small change in the latitude. Consequently, the variation with receiver longitude plotted in Fig. 8 corresponds to a nearly constant latitude.) For the cases shown in Figs. 7 and 8, the starting direction (δ_φ, δ_θ) of each initial ray of the triad of rays, and the incremental step sizes ($d\delta_\varphi$,$d\delta_\theta$) were inserted by having separate cards read by the computer.

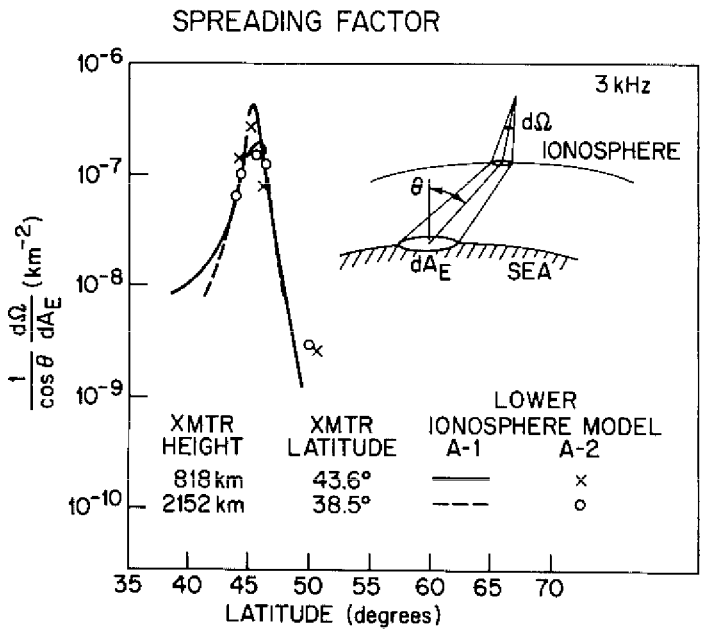

Fig. 7 — Variation of spreading factor with receiver latitude for two fixed transmitter locations. The X's and O's are results for lower ionospheric model A-2. The lines are results for model A-1.

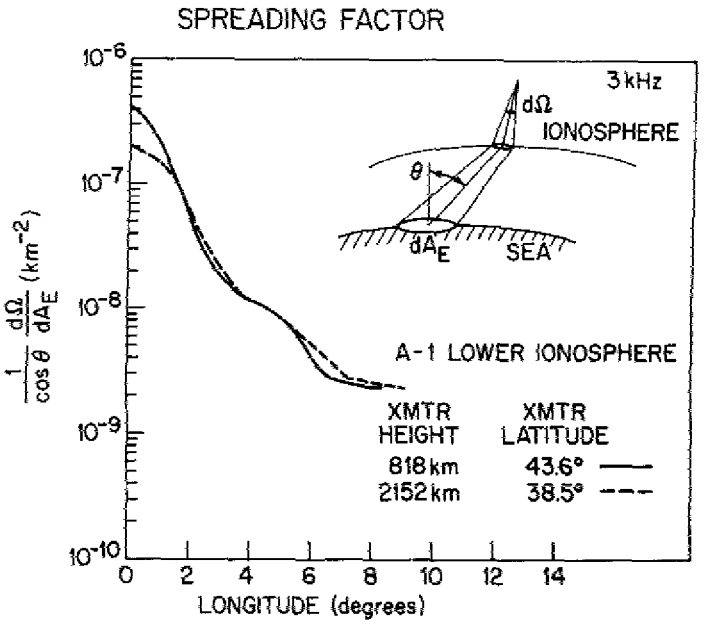

Fig. 8 — Variation of spreading factor with receiver longitude for two fixed transmitter locations. Model A-1 results are shown.

After data for Figs. 7 and 8 were obtained, the program was modified to provide an automatic choice of δ_θ, δ_φ, $d\delta_\theta, d\delta_\varphi$ for efficiently implementing subsequent calculations. With this procedure the results of Figs. 9 through 13 were obtained using various lower ionosphere models. Multiple hop spreading factors were also obtained using this automatic procedure. Plots of the lognitudinal variations of the spreading factor for the multihop case for transmitter frequencies of 3kHz and 10kHz are shown in Figs. 14 and 15, respectively.

DISCUSSION

Spreading Factor

Figures 7 through 10 imply that, for fixed low-altitude transmitter locations, the received field at the earth's surface is a very sensitive function of the receiver location. For example, if the receiver is 3° from the maximum spreading factor point of the "hot-spot" area, the signal may be reduced by as much as 10 dB.

Figures 9 and 10 show that the spreading factor depends on the selection of the lower ionospheric model. It is thought that the suppression of the latitude dependence of the lower ionospheric layers when model A-1 is used may account for the differences in the calculated spreading factors.

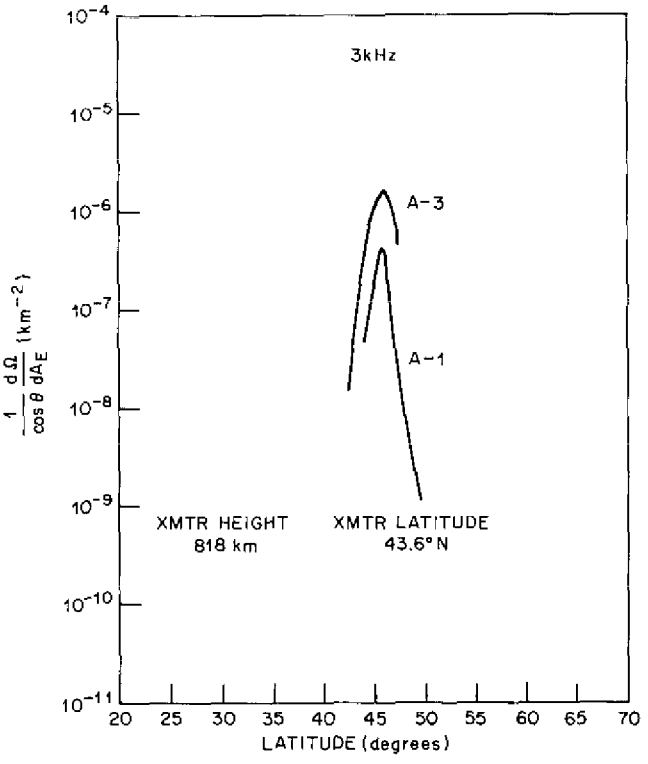

Fig. 9 — Comparison of latitude variation of spreading factor using models A-1 and A-3

Figures 11 and 12 compare the spreading factors of two transmitters located near the magnetic equator to those of one located at midlatitude at 303-km height. Figure 13 shows some of the ray traces used in producing Fig. 11. The higher equatorial transmitter produces a pattern (curve b, Fig. 11) which is much lower in magnitude and broader in latitude than that (curve a) of the lower altitude transmitter. The pattern of the higher equatorial satellite also appears to be much smaller in longitudinal extent (approximately 7°), than in latitudinal extent (approximately 17°). The lower equatorial satellite (curve c) does not produce such a broad latitudinal coverage pattern, nor is there as much difference between its latitudinal and longitudinal coverage patterns. The magnetospheric plasma density model contains a latitudinal variation which, as shown in Fig. 3, causes a relatively complicated focusing and defocusing of rays that originate at different latitudes and altitudes. The plasma model effects appear to be reflected here in the difference in coverage patterns by transmitters located at different heights above the magnetic equator.

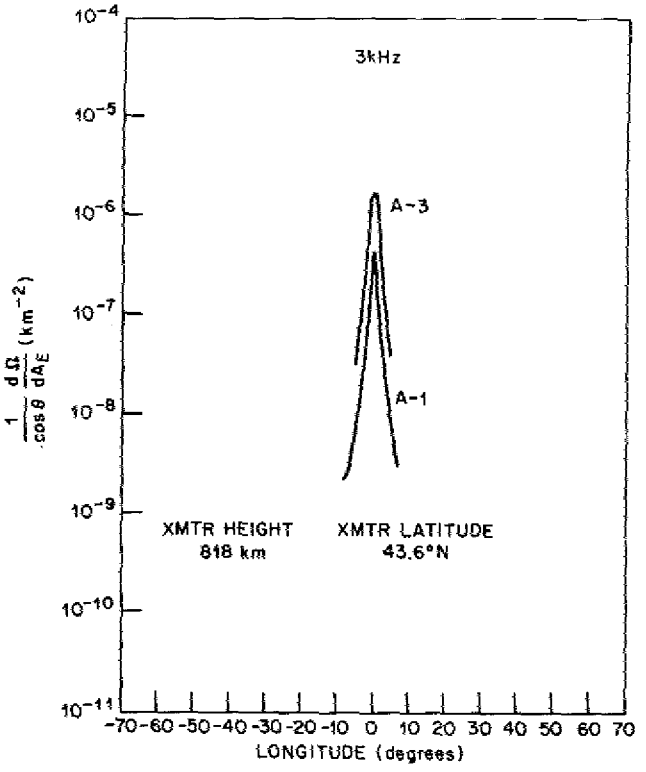

Fig. 10 — Comparison of longitude variation of spreading factor using models A-1 and A-3

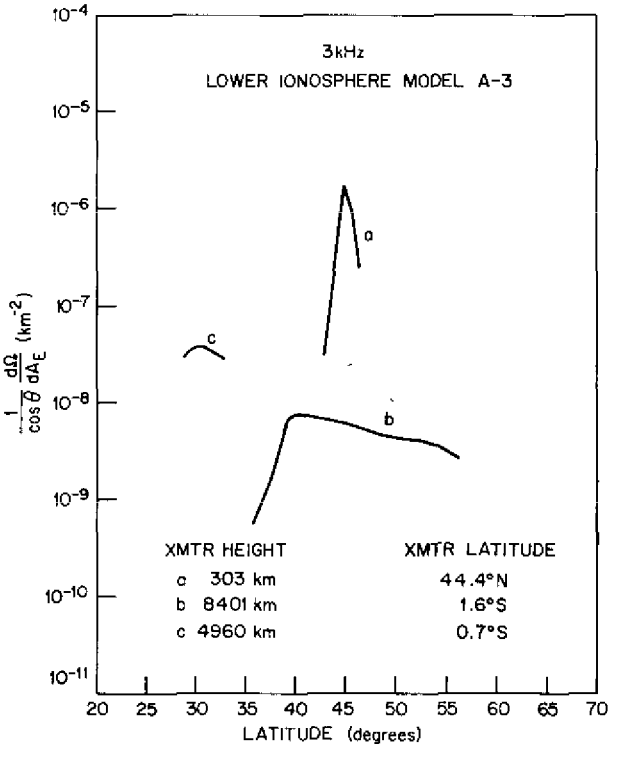

Fig. 11 — Latitude variation of spreading factor for various conditions: (a) transmitter slightly below F-layer; (b) and (c) high-altitude transmitters located near equator. Model A-3 was used.

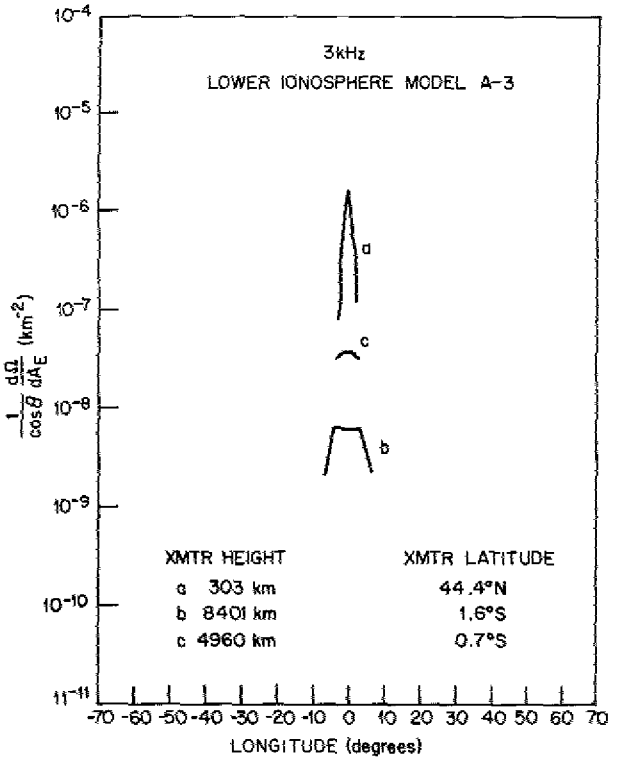

Fig. 12 — Longitude variation of spreading factor for various conditions: (a) transmitter slightly below F-layer; (b) and (c) high-altitude transmitters located near equator. Model A-3 was used.

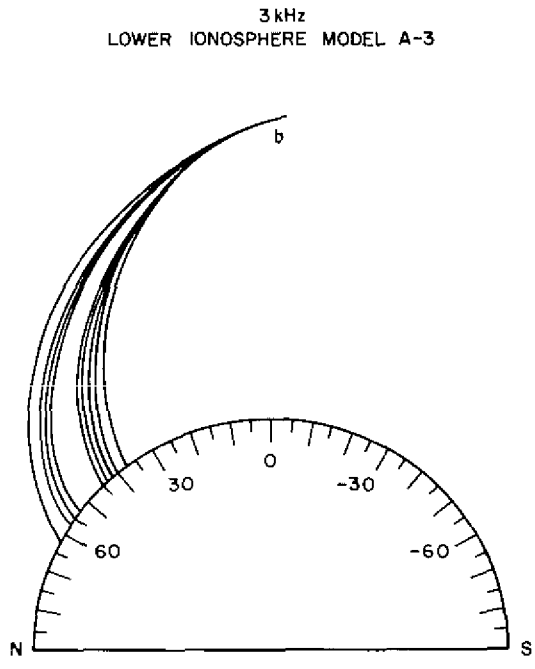

Fig. 13 — Ray traces used to obtain spreading factors shown in Fig. 11 for case b

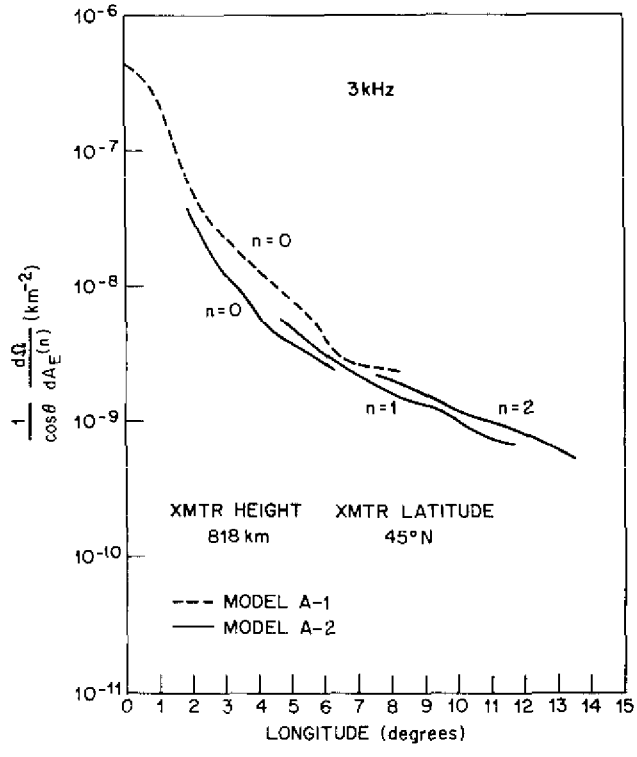

Fig. 14 — Longitudinal variation of multihop spreading factors at 3 kHz using models A-1 and A-2 ionospheres

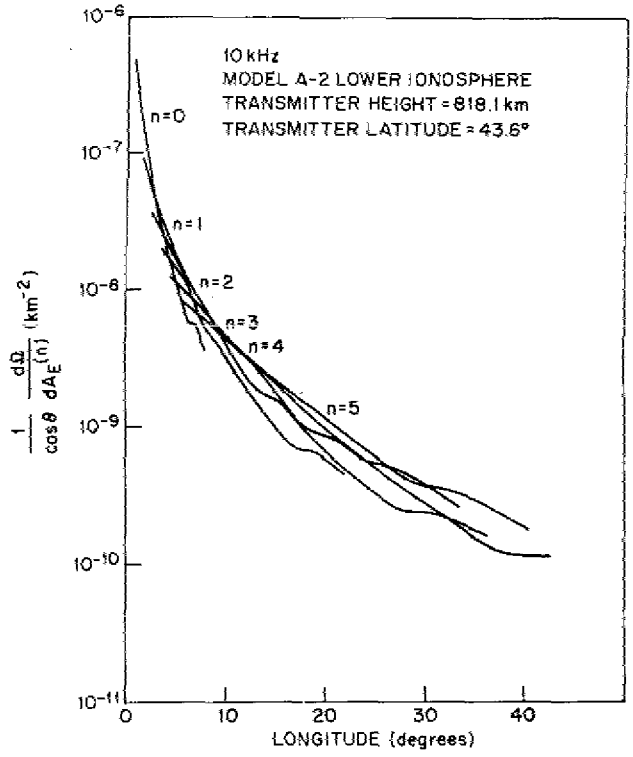

Fig. 15 — Longitudinal variation of multihop spreading factors at 10 kHz using model A-2 ionosphere

Smith and Rorden Comparison

Smith and Rorden [17] have presented an approximate equation for the signal power budget of an ELF/VLF transmitting satellite. They use a factor (Eq. (18)) that is analogous to our spreading term appropriate for the maximum signal point of the hot spot

$$\frac{1}{\cos\theta}\frac{d\Omega^{(o)}}{dA_E} = \frac{1}{\mu^2 h^2} \tag{18}$$

where μ is the index of refraction of the wave at the satellite, and h is the height of the earth-ionosphere waveguide.

Table 1 presents a comparison of results using Eq. (18) and our results using ray tracing techniques. The appropriate value of μ was obtained from the ray tracing output. From the cases shown in Table 1 we see that the values of the Smith-Rorden spreading factor fall in the range of values predicted by ray tracing techniques, but differences between the factors by as much as a factor of 3 occur. Further, Eq. (18) predicts that the spreading factor should increase as the satellite location is changed from (818 km, 43.6°N) to (2152 km, 38.5°N). In fact, the spreading factor decreases. These differences

Table 1
Comparison of the 3-kHz Geometrical Spreading Factor
with the Approximate Value of Smith and Rorden

Transmitter Coordinates		Lower Ionosphere Model	Eq. (18) Prediction* (km^{-2})	Our Prediction $km^{(-2)}$
Height (km)	Latitude			
818	43.6°N	A-1	6.8×10^{-7}	4.3×10^{-7}
818	43.6°N	A-2	4.7×10^{-7}	2.8×10^{-7}
818	43.6°N	A-3	4.6×10^{-7}	1.77×10^{-6}
2152	38.5°N	A-1	8.95×10^{-7}	2.0×10^{-7}
2152	38.5°N	A-2	6.21×10^{-7}	1.6×10^{-7}

*For comparisons to our prediction using Models A-1, A-2 and A-3, we have used heights h of 70, 84, and 70 km, respectively, in Eq. (18).

occur, in part, because Eq. (18) ignores any spreading occurring during propagation from the satellite to the lower ionosphere boundary.

Multihop Spreading Factors

Figures 14 and 15 show the results of multihop evaluations of the spreading factor. We note that near the center of the spreading factor pattern the direct path spreading factor is the largest; but as the receiver location moves away from this central location the spreading factors of rays having one, two, and then three, etc., reflections from the ionosphere are largest in their turn.

CONCLUSIONS

Single and multiple hop spreading factors have been evaluated for a number of cases. In all low altitude transmitter cases the spreading factor decreased rapidly in magnitude as distance from the maximum point of the hot spot power pattern increased. The spreading factor pattern is shown to depend on the lower ionospheric model used for calculations. The spreading factor is shown to be smaller and less sensitive to receiver location for a fixed high altitude transmitter location. Qualitative and quantitative differences exist between our spreading factor results and those obtained using an expression of Smith and Rorden.

ACKNOWLEDGMENTS

We wish to thank B. Wald, W. Ament, W. E. Garner, and L. S. Bearce for their encouragement and advice. We wish to thank P. H. Alexander and M. Rycroft for a helpful communication. We wish to thank R.N. DeWitt for his help in composing some of the figures used in this report.

REFERENCES

1. V. L. Ginzburg, *Propagation of Electromagnetic Waves in Plasma*, Gordon and Breach, New York, 1961.

2. L. B. Felsen and N. Marcuvitz, *Radiation and Scattering of Waves*, Prentice-Hall, Englewood Cliffs, N. J., 1973.

3. L. M. Brekhovskikh, *Waves in Layered Media*, Academic Press, New York, 1960.

4. M. Born and E. Wolf, *Principles of Optics*, 4th ed., Pergamon Press, London, 1970.

5. J. Galejs, *Terrestrial Propagation of Long Electromagnetic Waves*, Pergamon Press, Oxford, 1972.

6. J. R. Wait, *Electromagnetic Waves in Stratified Media*, Pergamon Press, New York, 1962.

7. A. D. Watt, *VLF Radio Engineering*, Pergamon Press, Oxford, 1967.

8. R. A. Helliwell, *Whistlers and Related Ionospheric Phenomena*, Stanford University Press, Stanford, California, 1965.

9. J. H. Crary, "The Effect of the Earth-Ionosphere Waveguide on Whistlers," Technical Report No. 9, Stanford Electronics Laboratories, Stanford University, July 17, 1961, AD 262348.

10. R. L. Heyborne, "Observations of Whistler-Mode Signals in the OGO Satellites from VLF Ground Station Transmitters," Technical Report No. 3415/3418-1, Stanford Electronics Laboratories, Stanford University, 1966.

11. H. Bremmer, *Terrestrial Radio Waves: Theory of Propagation*, Elsevier Publishing Company, Amsterdam, 1949.

12. P. D. Alexander, "Computation of Ray Paths for Very Low Frequency Radio Waves Propagating Through the Magnetospheric Plasma," Ph.D. Thesis, University of Southhampton, April 1971.

13. J. Haselgrove, "Ray Theory and a New Method for Ray Tracing," in *Report of the Physical Society Conference on the Physics of the Ionosphere*, Physical Society, London, 1955, p. 355.

14. K. G. Budden, *Radio Waves in the Ionosphere: The Mathematical Theory of the Reflection of Radio Waves from Stratified Ionised Layers*, Cambridge University Press, 1961.

15. S. Gill, "A Process for the Step-by-Step Integration of Differential Equations in an Automatic Digital Computing Machine," Cambridge Phil. Soc. Proc. 47, Part I, 96-108 (Jan. 1951).

16. T. H. Stix, *The Theory of Plasma Waves*, McGraw-Hill, New York, 1962.

17. L. H. Rorden, R. L. Smith, and L. C. Bacon, "Sub-LF Satcom Technology Development Program," Report No. 532-720731 (Secret Report, Unclassified Title), Develco, Inc., Mountain View, Calif., 1972.

Appendix

LOWER IONOSPHERIC MODELS

The three lower ionospheric models that were used to produce the spreading factor results shown in this report are described in this appendix.

LINEAR LOWER IONOSPHERIC MODEL

Model A-1, the linear lower ionospheric model, is rather simple in form. The electron and ion densities are selected so that they diminish linearly with height between 300 and 70 km. The particle densities at 300 km are fixed by the computer to be equal to the particle density of the magnetospheric model at the point where the ray crosses the 300-km level. The linear variation of particle density with height is then fixed so that the densities would equal zero particles per cubic centimeter at a 70-km height. The particle densities are fixed so as not to vary in latitude or longitude once the ray passes below 300 km.

LOWER IONOSPHERIC MODEL A-2

In model A-2 the electron density variation with height is more complicated and hopefully more realistic.* As with model A-1, the electron and ion densities at 300 km are set equal to the densities of the magnetospheric model at the point where the ray crosses the 300-km level. The ion densities are set to decrease linearly from their values at 300 km down to zero at 68-km height. The electron density varies with height in a more complicated way. The electron density profile is divided into six layers. In each layer the electron density $N(h)$ is calculated by an expression of the form

$$N(h) = N_0 \, 10^{a_0 + a_1 \, h + a_2 h^2 + a_3 h^3} , \qquad \text{(A1)}$$

where N_0 is an overall normalizing parameter for each layer; a_0, a_1, a_2, and a_3 are chosen to fit a model ionosphere; and h is the height of the point above the ground. The N_0 parameter of each layer is chosen to make the electron density variation continuous with height in proceeding from a higher layer to a lower one. In the layer between 100.0- and 95.0-km height, a linear variation of electron density with height is assumed. In the layer below this linear variation, N_0 is set equal to 1.0. Below 84.0 km the electron and ion densities are all set to zero. The electron and ion densities are not permitted to vary with latitude or longitude below 300 km.

*J. Galejs, "Stable Solutions of Ionospheric Fields in the Propagation of ELF and VLF Waves," Radio Sci. 7, 549-561 (1972).

Figure A1 shows typical electron density profiles from models A-1 and A-2. Table A1 presents a list of the layer boundary heights and the values of the $\{a_i\}$ within these layers for model A-2.

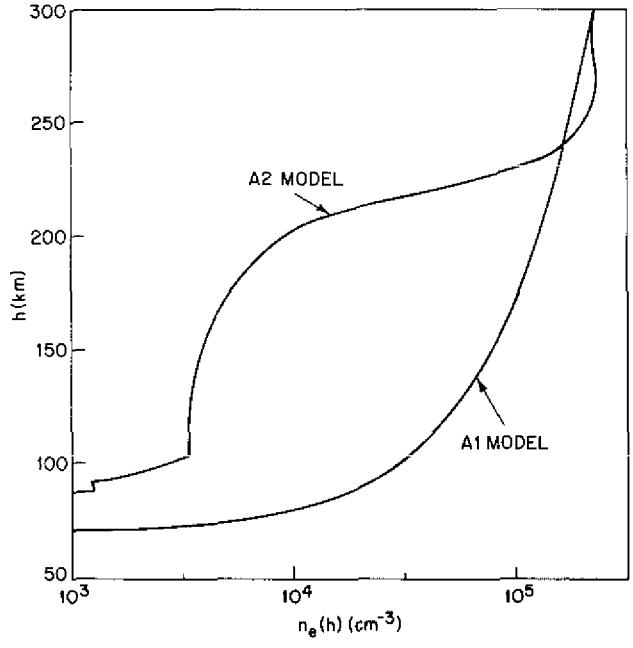

Fig. A1 — Graphs showing typical electron density profiles for models A-1 and A-2

SMOOTHLY VARYING LOWER IONOSPHERIC MODEL A-3

Ionospheric model A-3 is a latitude-dependent model having a smoothly varying electron density profile. It is joined to the magnetospheric model at the reference height of 900 km. Below 900 km the relative ion abundance ratios along each geomagnetic field line are fixed at their reference height values.

The electron density profile for model A-3 is divided into a number of concentric layers. In each layer the electron density N is calculated using an expression of the form

$$N(h,\theta) = N_{900}^{a_0 + a_1 s + a_2 s^2 + a_3 s^3 + a_4 s^4} \tag{A2}$$

where N_{900} is the electron density at the reference height along the field line passing through the point given by altitude h and latitude θ. The normalized height s is defined by

Table A1
Values of the $\{a_i\}$ used in Producing Model A-2

Layer Number	Layer Heights (km)		a_0	a_1	a_2	a_3
	Top	Bottom				
1	300	240	-6.341346×10^{1}	7.382568×10^{-1}	-2.651159×10^{-3}	3.168195×10^{-6}
2	240	200	3.118793×10^{2}	-4.295851	1.978827×10^{-2}	-3.007970×10^{-5}
3	200	100	2.605656	1.544002×10^{-2}	-1.429726×10^{-4}	4.528743×10^{-7}
4	100	95				
5	95	85	-7.724051×10^{2}	2.617383×10^{1}	-2.944590×10^{-1}	1.103716×10^{-3}
6	85	84	-2.318612×10^{3}	8.991779×10^{1}	-1.161261	4.996458×10^{-3}

$$s \equiv (h - h_a) / (900 - h_a)$$

with h_a equal to the lower boundary height of the ionosphere. Table A2 lists the layer boundary heights and the values of the coefficients $\{a_i\}$ within each layer for model A-3. The coefficients were chosen to closely approximate observed electron density profiles from the F layer peak to 900 km and to provide a smooth transition from this peak to the low electron densities observed near the bottom of the ionosphere. Figure A2 shows the variation of the normalized electron density along a field line as a function of altitude.

Because the normalization constant $\log_{10}N_{900}$ appearing in Fig. A2 is latitude dependent, the actual electron density vs height profile varies from one field line to another in this model.

Table A2
Values of the $\{a_i\}$ used in Producing Model A-3

Layer Number	Layer Heights (km)		a_0	a_1	a_2	a_3	a_4
	Top	Bottom					
1	111.5	70	0.00000	18.60000	488.2222	-12768.8888	60088.88888
2	194.5	111.5	0.85930	0.99233	11.4155	-65.0222	107.55555
3	319	194.5	1.36084	-7.13689	52.166	-118.8938	73.50349
4	900	319	1.10995	1.45814	-3.4423	2.4989	-0.62473

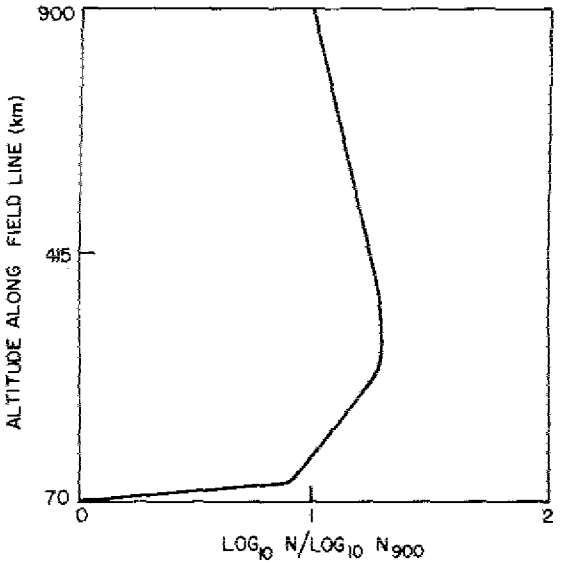

Fig. A2 — Graph showing typical electron density profile along field lines for model A-3